

Towards Visible Soliton Microcomb Generation

Seung Hoon Lee^{1*}, Dong Yoon Oh^{1*}, Qi-Fan Yang^{1*}, Boqiang Shen^{1*}, Heming Wang^{1*},
Ki Youl Yang¹, Yu Hung Lai¹, Xu Yi¹, and Kerry Vahala^{1†}

¹T. J. Watson Laboratory of Applied Physics, California Institute of Technology, Pasadena, California 91125, USA.

*These authors contributed equally to this work.

†Corresponding author: vahala@caltech.edu

Frequency combs have applications that extend from the ultra-violet into the mid infrared bands. Microcombs¹, a miniature and often semiconductor-chip-based device, can potentially access most of these applications, but are currently more limited in spectral reach. Here, we demonstrate mode-locked silica microcombs with emission near the edge of the visible spectrum. By using both geometrical and mode-hybridization dispersion control, devices are engineered for soliton generation while also maintaining optical Q factors as high as 80 million. Electronics-bandwidth-compatible (20 GHz) soliton mode locking is achieved with threshold powers as low as 5.4 mW. These are the shortest wavelength soliton microcombs demonstrated to date and could be used in miniature optical-clocks^{2,3}. The results should also extend to visible and potentially ultraviolet bands.

Soliton microcombs⁴⁻⁸ provide a pathway to miniaturize many conventional comb applications. They have also opened investigations into new nonlinear physics associated with dissipative Kerr solitons⁴ and Stokes solitons⁹. In contrast to early microcombs, soliton microcombs eliminate instabilities, provide stable (low-phase-noise) mode locking and feature a highly reproducible spectral envelope. Many applications of these devices are being studied including chip-based optical frequency synthesis¹⁰, secondary time standards³ and dual-comb spectroscopy¹¹⁻¹³. Also, a range of operating wavelengths is opening up by use of several low-optical-loss dielectric materials for resonator fabrication. In the near-infrared (IR), microcombs based on magnesium fluoride⁴, silica^{5,14} and silicon nitride^{6-8,15,16} are being studied for frequency metrology and frequency synthesis. In the mid-IR spectral region silicon nitride¹⁷, crystalline¹⁸, and silicon-based¹⁹ Kerr microcombs as well as quantum-cascade microcombs²⁰ are being studied for application to molecular fingerprinting.

At shorter wavelengths below 1 μm , microcomb technology would benefit optical atomic clock technology²¹, particularly efforts to miniaturize these clocks. For example, microcomb optical clocks based on the D1 transition (795 nm) and the two-photon clock transition²² (798 nm) in rubidium have been proposed^{2,3}. Also, a microcomb clock using two-point locking to rubidium D1 and D2 lines has been demonstrated²³ by frequency doubling from the near-IR. More generally, microcomb sources in

the visible and ultraviolet bands could provide a miniature alternative to larger mode-locked systems such as titanium sapphire lasers in cases where high power is not required. It is also possible that these shorter wavelength systems could be applied in optical coherence tomography systems²⁴⁻²⁶. Efforts directed towards short wavelength microcomb operation include 1 μm microcombs in silicon nitride microresonators²⁷ as well as harmonically-generated combs. The latter have successfully converted near IR comb light to shorter wavelength bands²⁸ and even into the visible band^{29,30} within the same resonator used to create the initial comb of near-IR frequencies. Also, crystalline resonators³¹ and silica microbubble resonators³² have been dispersion-engineered for comb generation in the 700 nm band. Finally, diamond-based microcombs afford the possibility of broad wavelength coverage³³. However, none of the short wavelength microcomb systems have so far been able to generate stable mode-locked microcombs as required in all comb applications.

A key impediment to mode-locked microcomb operation at short wavelengths is material dispersion associated with the various dielectric materials used for microresonator fabrication. At shorter wavelengths, these materials feature large normal dispersion that dramatically increases into the visible and ultraviolet bands. Soliton-based mode-locking, on the other hand, requires anomalous dispersion. Dispersion engineering by proper design of the resonator geometry^{2,31,32,34-39} offers a possible way to offset the normal dispersion. Typically, by compressing a resonator's waveguide dimension, geometric dispersion will ultimately compensate a large normal material dispersion component to produce overall anomalous dispersion. For example, in silica, strong confinement in bubble resonators³² and straight waveguides⁴⁰ has been used to push the anomalous dispersion transition wavelength from the near-IR into the visible band. Phase matching to ultraviolet dispersive waves has also been demonstrated using this technique⁴⁰. However, to compensate the rising material dispersion this compression must increase as operational wavelength is decreased, and as a side effect highly-confined waveguides tend to suffer increased optical losses. This happens because mode overlap with the dielectric waveguide interface is greater with reduced waveguide cross section. Consequently, the residual fabrication-induced roughness of that interface degrades the resonator Q factor and increases pumping power (i.e., comb threshold power varies

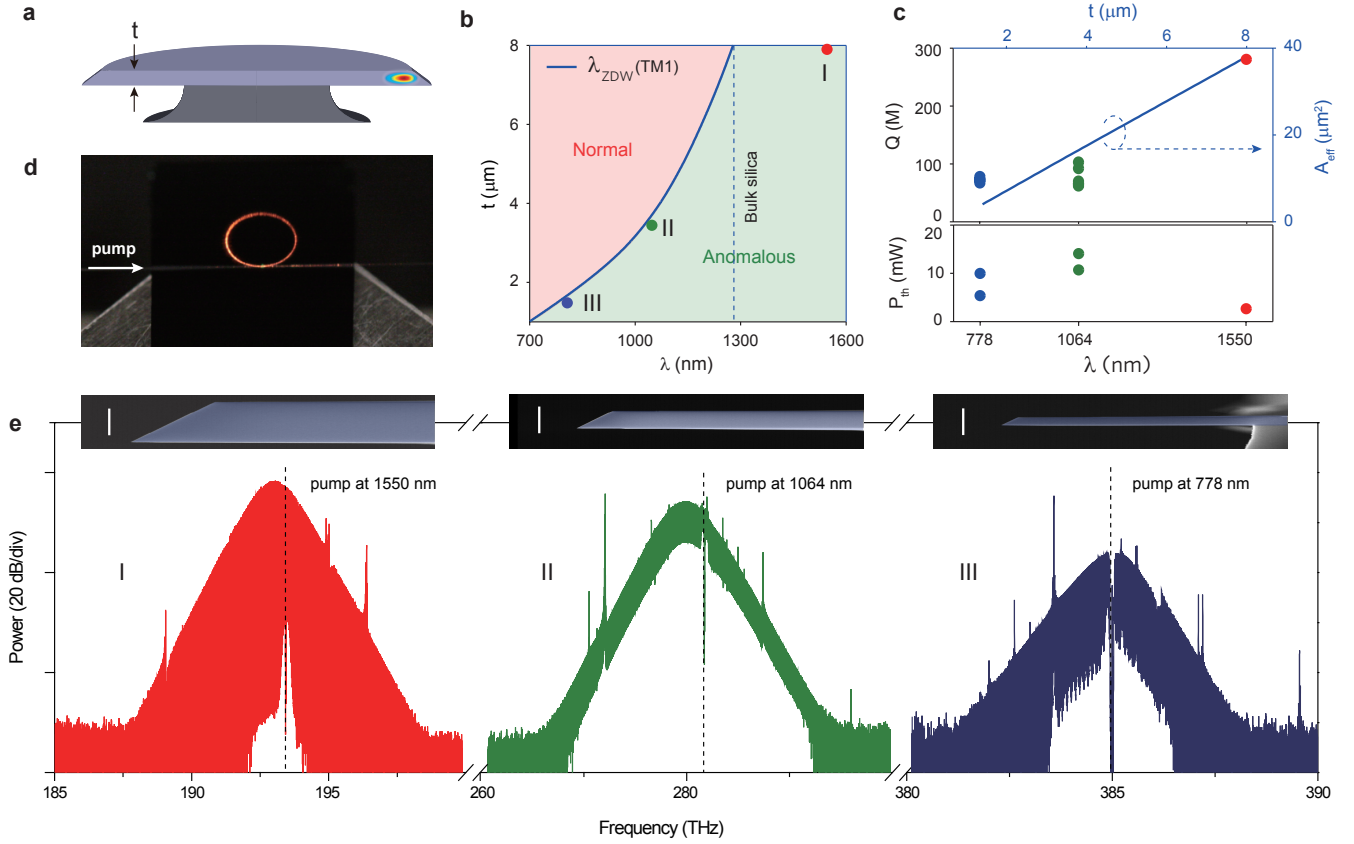


FIG. 1: Soliton frequency comb generation in dispersion-engineered silica resonators. (a) A rendering of a silica resonator with the calculated mode profile of the TM1 mode superimposed. (b) Regions of normal and anomalous dispersion are shown versus silica resonator thickness (t) and pump wavelength. The zero dispersion wavelength (λ_{ZDW}) for the TM1 mode appears as a blue curve. Plot is made for a 3.2-mm-diameter silica resonator. Three different device types I, II, and III (corresponding to three oxide thicknesses) are indicated for soliton generation at 1550 nm, 1064 nm and 778 nm. (c) Measured Q factors and comb threshold powers versus thickness and pump wavelength for the three device types. Effective mode area (A_{eff}) of the TM1 mode family is also plotted as a function of wavelength and thickness. (d) A photograph of a silica resonator (Type III device pumped at 778 nm) while generating a soliton stream. The pump light is coupled via a tapered fiber from the left side of the resonator. The red light along the circumference of the resonator and at the right side of the taper is due to the short wavelength components of the soliton comb. (e) Soliton frequency comb spectra measured using device types I, II, and III designed for pump wavelengths 1550 nm, 1064 nm, and 778 nm, respectively. Pump frequency location is indicated by a dashed vertical line. The soliton pulse repetition rate of all devices is about 20 GHz. Insets: cross-sectional SEM images of the fabricated resonators. White scale bar is 5 μm .

inverse quadratically with Q factor⁴¹).

Minimizing material dispersion provides one way to ease the impact of these constraints. In this sense, silica offers an excellent material for short wavelength operation, because it has the lowest dispersion among all on-chip integrable materials. For example, at 778 nm, silica has a group velocity dispersion (GVD) equal to 38 ps^2/km , which is over 5X smaller than the GVD of silicon nitride at this wavelength ($> 200 \text{ps}^2/\text{km}$)⁴². Other integrable materials that are also transparent in the visible, such as diamond³³ and aluminum nitride⁴³, have dispersion that is similar to or higher than silicon nitride. Silica also features a spectrally-broad low-optical-loss win-

dow so that optical Q factors can be high at short wavelengths. Here we demonstrate soliton microcombs with pump wavelengths of 1064 nm and 778 nm. These are the shortest soliton microcomb wavelengths demonstrated to date. By engineering geometric dispersion and by employing mode hybridization, net anomalous dispersion has been achieved at these wavelengths while also maintaining high optical Q factors (80 million at 778 nm, 90 million at 1064 nm). The devices have large (millimeter-scale) diameters and produce single soliton pulse streams at rates that are both detectable and processible by low-cost electronic circuits. Besides illustrating the flexibility of silica for soliton microcomb generation across a

range of short wavelengths, these results are relevant to potential secondary time standards based on transitions in rubidium^{2,3,23}. Using dispersive-wave engineering in silica it might also be possible to extend the emission of these combs into the ultraviolet as recently demonstrated in compact silica waveguides⁴⁰.

The silica resonator used in this work is shown schematically in Fig. 1a. A fundamental mode profile is overlaid in the cross-sectional rendering. As described in detail below, the resonator thickness (t) is controlled to obtain net anomalous dispersion at the design wavelengths. The resonator design is a variation on the wedge resonator⁴⁴ and precise thickness control (t -control) is possible because this layer is formed through oxidation of a silicon wafer. The diameter of all resonators in this work (and the assumed diameter in all simulations) is 3.2 mm, which corresponds to a free-spectral-range (FSR) of approximately 20 GHz. Further details on fabrication are given elsewhere⁴⁴. As an aside, we note that a waveguide-integrated version of this design is also possible⁴⁵. Adaptation of that device using the methods described here would enable full integration with other photonic elements on the silicon chip.

Fig. 1b illustrates the dispersion design space by showing regions of anomalous and normal dispersion for the TM1 mode family versus resonator thickness t and pumping wavelength. The plot shows that as the pump wavelength decreases the resonator needs to be thinner to access the anomalous dispersion regime. With this in mind, we have selected three different device types for soliton frequency comb operation at three different pump wavelengths. These are indicated in Fig. 1b as I, II and III with colored dots. At a pump wavelength of 1550 nm, the anomalous dispersion window is wide because bulk silica possesses anomalous dispersion at wavelengths above 1270 nm. For this device (Type I), an 8- μm thickness was used. Devices of type II and III have thicknesses near 3.5 μm and 1.5 μm for operation with pump wavelengths of 1064 nm and 778 nm, respectively. Measured Q factors for the three device types are plotted in the upper panel of Fig. 1c. Maximum Q factors at thicknesses which also produce anomalous dispersion were: 280 million (Type I, 1550 nm), 90 million (Type II, 1064 nm) and 80 million (Type III, 778 nm).

Using these three designs, soliton frequency combs were successfully generated with low threshold pump power. Shown in Fig. 1d is a photograph of a type III device. Soliton frequency components in the 700 nm band generate the red light in the photograph. Fig. 1e shows optical spectra of the soliton microcombs generated for each device type. A slight Raman-induced soliton self-frequency-shift is observable in the type I and type II devices^{5,46-48}. Scanning electron microscope (SEM) images appear as insets in Fig. 1e and provide cross-sectional views of the three device types. It is worthwhile to note that microcomb threshold power, expressed as $P_{th} \sim A_{eff}/\lambda_p Q^2$ (λ_p is pump wavelength and A_{eff} is effective mode area) remains within a close range of powers

for all devices (lower panel of Fig. 1c). This can be understood to result from partial compensation of reduced Q factor in the shorter wavelength devices by reduced optical mode area (see plot in Fig. 1c). For example, from 1550 nm to 778 nm the mode area is reduced by roughly a factor of 9 and this helps to offset a decrease in Q factor of 3X. The resulting P_{th} increase (5.4 mW at 778 nm versus approximately 2.5 mW at 1550 nm) is therefore caused primarily by the decrease in pump wavelength λ_p . In the following sections additional details on the device design, dispersion and experimental techniques used to generate these solitons are presented.

Dispersion simulations for TM modes near 1064 nm are presented in Fig. 2a and show that TM modes with anomalous dispersion occur in silica resonators having oxide thicknesses less than 3.7 μm . Aside from the thickness control, a secondary method to manipulate dispersion is by changing the wedge angle (see Fig. 2a). Here, wedge angles between 30 and 40 degrees were chosen in order to maximize the Q factors⁴⁴. The resonator dispersion is characterized by measuring mode frequencies using a scanning external-cavity-diode-laser (ECDL) whose frequency is calibrated using a Mach-Zehnder interferometer. As described elsewhere^{4,5} the mode frequencies, ω_μ , are Taylor expanded to second order as $\omega_\mu = \omega_o + \mu D_1 + \mu^2 D_2/2$, where ω_o denotes the pumped mode frequency and $D_1/2\pi$ is the FSR. D_2 is related to the GVD, β_2 , by $D_2 = -cD_1^2\beta_2/n_o$ where c and n_o are the speed of light and material refractive index, respectively. The measured frequency spectrum of the TM1 mode family in a 3.4 μm thick resonator is plotted in Fig. 2b. The plot gives the frequency as relative frequency (i.e., $\omega_\mu - \omega_o - \mu D_1$) to make clear the second-order dispersion contribution. Also shown is a fitted parabola (red curve) revealing $D_2/2\pi = 3.3$ kHz (positive parabolic curvature indicates anomalous dispersion). Some avoided mode crossings are observed in the spectrum. The dispersion measured in resonators of different thicknesses, marked as solid dots in Fig. 2a, is in good agreement with numerical simulations.

The experimental setup for generation of 1064 nm pumped solitons is shown in Fig. 2c. The microresonator is pumped by a CW laser amplified by a YDFA. The pump light and comb power are coupled to and from the resonator by a tapered fiber^{49,50}. Solitons are generated while scanning the laser from higher frequencies to lower frequencies across the pump mode⁴⁻⁶. The pump light is modulated by an electro-optic PM to overcome the thermal transient during soliton generation^{5,6,51}. A servo control referenced to the soliton power is employed to capture and stabilize the solitons⁵¹. Shown in Fig. 2d are the optical spectra of solitons pumped at 1064 nm. These solitons are generated using the mode family whose dispersion is characterized in Fig. 2b. Due to the relatively low dispersion (small D_2), these solitons have a short temporal pulsewidth. Using the hyperbolic-secant-squared fitting method (see orange and green curves in Fig. 2d) a soliton pulse width of 52 fs is estimated for

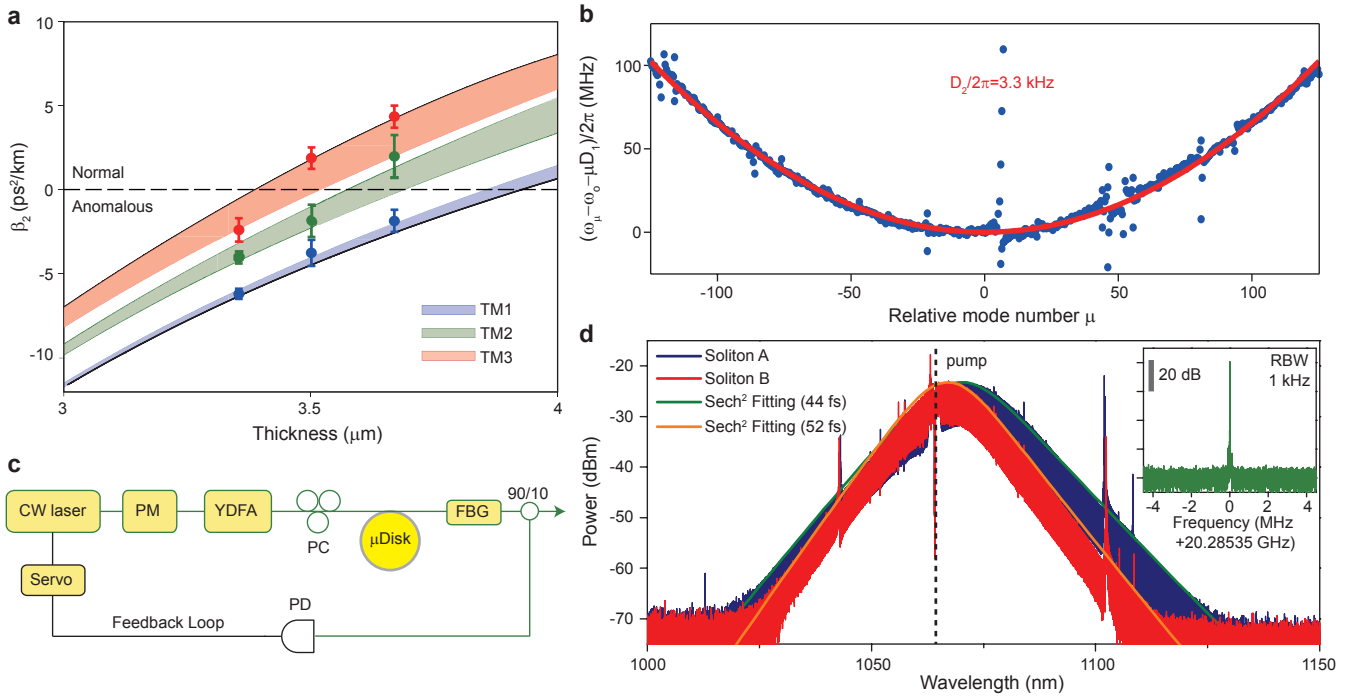


FIG. 2: **Microresonator dispersion engineering and soliton generation at 1064 nm.** (a) Simulated dispersion (GVD) of TM mode families versus resonator thickness. The angle of the wedge ranges from 30° to 40° in the colored regions. Measured data points are indicated and agree well with the simulation. (b) Measured relative mode frequencies (blue points) plotted versus relative mode number of a soliton-forming TM1 mode family in a $3.4 \mu\text{m}$ thick resonator. The red curve is a parabolic fit yielding $D_2/2\pi = 3.3$ kHz. (c) Experimental setup for soliton generation. A continuous-wave (CW) fiber laser is modulated by an electro-optic phase modulator (PM) before coupling to a ytterbium-doped-fiber-amplifier (YDFA). The pump light is then coupled to the resonator using a tapered fiber. Part of the comb power is used to servo-lock the pump laser frequency. FBG: fiber Bragg grating. PD: photodetector. PC: polarization controller. (d) Optical spectra of solitons at 1064 nm generated from the mode family shown in b. The two soliton spectra correspond to different power levels with the blue spectrum being a higher power and wider bandwidth soliton. The dashed vertical line shows the location of the pump frequency. The solid curves are sech^2 fittings. Inset: typical detected electrical beatnote showing soliton repetition rate. RBW: resolution bandwidth.

the red spectrum. By increasing the soliton power (blue spectrum) the soliton can be further compressed to 44 fs, which corresponds to a duty cycle of 0.09% at the 20 GHz repetition rate. Finally, the inset in Fig. 2d shows the electrical spectrum of the photodetected soliton pulse stream. Besides confirming the repetition frequency, the spectrum is very stable with excellent signal-to-noise ratio (SNR) greater than 70 dB at 1 kHz RBW.

For soliton operation near the pump wavelength 778 nm, a resonator thickness around $1.5 \mu\text{m}$ is chosen, which is close to the zero GVD of the TM1 mode (see Fig. 1b). Operation at this point provides thicker oxide and therefore higher optical Q factors. Under normal circumstances the near-zero GVD would prove challenging to control during fabrication, so mode coupling is used to further engineer the dispersion^{2,36,37,53}. Specifically, the anomalous dispersion of the TM1 mode is boosted through hybridization with the TE2 mode. As now shown, this mode hybridization is caused by two

factors: a degeneracy in the effective index at the pump wavelength of the two modes and a broken reflection symmetry of the resonator⁵⁴. Finite element method (FEM) simulation in Fig. 3a shows that at 778 nm the TM1 and TE2 modes are expected to have the same effective index at the thickness $1.48 \mu\text{m}$ when the resonator features a symmetry upon reflection through a plane that is both parallel to the resonator surface and that lies at the center of the of resonator. Such a symmetry exists when the resonator has vertical sidewalls or equivalently a wedge angle $\theta = 90^\circ$ in the current resonator design. A zoom-in of the effective index crossing is provided in Fig. 3b. In this symmetrical case, the two modes cross in the effective-index plot without hybridization. However, in the case of $\theta = 40^\circ$ (Fig. 3c), the symmetry is broken and the point of effective index degeneracy does not exist. Instead, near the resonator thickness $1.48 \mu\text{m}$, two hybrid modes exist and these modes experience an avoided crossing. The avoided crossing causes a sudden

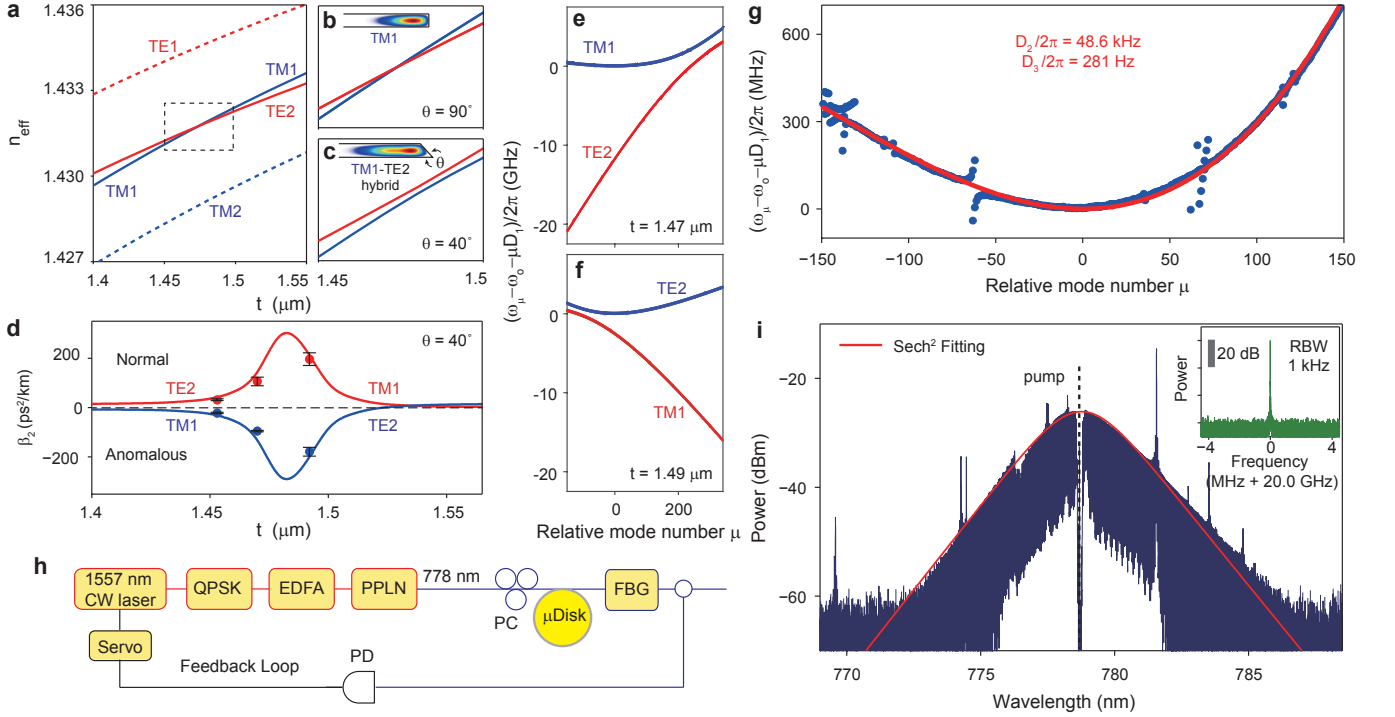


FIG. 3: Dispersion engineering and soliton generation at 778 nm. (a) Calculated effective indices for TE1, TE2, TM1, and TM2 modes at 778 nm plotted versus thickness for a silica resonator with reflection symmetry. The TM1 and TE2 modes cross each other without hybridization. The dashed box is the frame for the panel **b** zoom-in. (b) Zoom-in of the dashed box in panel **a**. Inset shows resonator with reflection symmetry (equivalent to wedge angle $\theta = 90^\circ$). (c) As in **b** but for resonator with $\theta = 40^\circ$. An avoided crossing of TM1 and TE2 occurs due to mode hybridization. (d) Calculated GVD of the two hybrid modes for $\theta = 40^\circ$. Hybridization causes a transition in the dispersion around the thickness 1.48 μm . The points are the measured dispersion values. (e, f) Measured relative mode frequencies of the TM1 and TE2 mode families versus relative mode number μ for devices with $t = 1.47 \mu\text{m}$ and $t = 1.49 \mu\text{m}$. (g) Zoom-in of panel **e** for the TM1 mode family. The red curve is a fit with $D_2/2\pi = 48.6 \text{ kHz}$ and $D_3/2\pi = 281 \text{ Hz}$. (h) Experimental setup for soliton generation. A 1557 nm tunable laser is sent to a quadrature phase shift keying modulator (QPSK) to utilize frequency-kicking⁵² and is then amplified by an erbium-doped-fiber-amplifier (EDFA). Then, a periodically poled lithium niobate (PPLN) waveguide frequency doubles the 1557 nm input into 778 nm output. The 778 nm pump light is coupled to the resonator for soliton generation. A servo loop is used to maintain pump locking⁵¹. (i) Optical spectrum of a 778 nm soliton with pump line indicated. The red curve is a spectral fitting which reveals the pulse width of 145 fs. Inset shows the electrical spectrum of the detected soliton pulse stream.

transition in the calculated group velocity dispersion as shown in Fig. 3d. One of the hybrid modes experiences enhanced anomalous dispersion.

To verify this effect, resonators with three different thicknesses were fabricated and their dispersion was characterized using the same method as for the 1064 nm soliton device. The measured second-order dispersion values are plotted as solid circles in Fig. 3d for comparison with the calculated values. In addition to second-order dispersion, the mode spectra of the two modes feature significant higher-order dispersion (β_3 and β_4) around the thickness 1.48 μm . Fig. 3e and Fig. 3f show the measured relative mode frequencies versus mode number of the two modes for devices with $t = 1.47 \mu\text{m}$ and $t = 1.49 \mu\text{m}$, respectively. A zoom-in of the TM1 mode spectrum for $t = 1.47 \mu\text{m}$ with a fit which includes third-

order dispersion (red curve) is shown in Fig. 3g. Despite the third-order dispersion, this dispersion curve is well suited for soliton formation.

For soliton generation, the microresonator is pumped at 778 nm by frequency-doubling from a CW ECDL operating at 1557 nm (see Fig. 3h). The 1557 nm laser is modulated by a QPSK modulator for frequency-kicking⁵² and then amplified by an EDFA. The amplified light is sent into a PPLN device for second-harmonic generation. The frequency-doubled output pump power at 778 nm is coupled to the microresonator using a tapered fiber. The soliton capture and locking method was again used to stabilize the solitons⁵¹. The optical spectrum of a 778 nm pumped soliton is shown in Fig. 3i. It features a temporal pulse width of 145 fs as derived from a sech² fit (red curve). The electrical spectrum of the photode-

tected soliton stream is provided as the inset to Fig. 3i and exhibits high stability.

In summary, we have demonstrated soliton microcombs at 778 nm and 1064 nm using on-chip high-Q silica resonators. Material-limited normal dispersion, which is dominant at these wavelengths, was compensated by using geometric dispersion through control of the resonator thickness and wedge angle. At the shortest wavelength, 778 nm, mode hybridization was also utilized to achieve anomalous dispersion while maintaining high optical Q. These results are the shortest wavelength soliton microcombs demonstrated to date. The generated solitons have pulse repetition rates of 20 GHz at both wavelengths. Such detectable and electronics-compatible repetition rate soliton microcombs at short wavelengths have direct applications in the development of miniature optical clocks^{2,3,23} and potentially optical coherence tomography^{24–26}. Also, any application requiring low-power near-visible mode-locked laser sources will benefit. The same dispersion control methods used here should be transferable to silica ridge resonator designs that contain silicon nitride waveguides for on-chip coupling

to other photonic devices⁴⁵. Also, it could be possible to design devices that use solitons formed at either 778 nm or 1064 nm for dispersive-wave generation into the visible and potentially into the ultraviolet as has been recently demonstrated using straight silica waveguides⁴⁰.

Acknowledgment The authors thank Scott Diddams and Andrey Matsko for helpful comments on this work. The authors gratefully acknowledge the Defense Advanced Research Projects Agency under the ACES program (Award No. HR0011-16-C-0118) and the SCOUT program (Award No. W911NF-16-1-0548). The authors also thank the Kavli Nanoscience Institute.

Author contributions SHL, DYO, QFY, BS, HW and KV conceived the experiment. SHL fabricated devices with assistance from DYO, BS, HW and KYY. DYO, QFY, BS and HW tested the resonator structures with assistance from SHL, KYY, YHL and XY. SHL, DYO, QFY, BS and HW modeled the device designs. All authors analyzed the data and contributed to writing the manuscript.

-
- ¹ Kippenberg, T. J., Holzwarth, R. & Diddams, S. A. Microresonator-based optical frequency combs. *Science* **332**, 555–559 (2011).
 - ² Soltani, M., Matsko, A. & Maleki, L. Enabling arbitrary wavelength frequency combs on chip. *Laser & Photonics Reviews* **10**, 158–162 (2016).
 - ³ Frank, I. *et al.* A low-power, chip-scale optical atomic clock with enhanced stability. In *Joint Navigation Conference* (2017).
 - ⁴ Herr, T. *et al.* Temporal solitons in optical microresonators. *Nature Photonics* **8**, 145–152 (2014).
 - ⁵ Yi, X., Yang, Q.-F., Yang, K. Y., Suh, M.-G. & Vahala, K. Soliton frequency comb at microwave rates in a high-Q silica microresonator. *Optica* **2**, 1078–1085 (2015).
 - ⁶ Brasch, V. *et al.* Photonic chip-based optical frequency comb using soliton cherenkov radiation. *Science* **351**, 357–360 (2016).
 - ⁷ Wang, P.-H. *et al.* Intracavity characterization of microcomb generation in the single-soliton regime. *Optics Express* **24**, 10890–10897 (2016).
 - ⁸ Joshi, C. *et al.* Thermally controlled comb generation and soliton modelocking in microresonators. *Optics Letters* **41**, 2565–2568 (2016).
 - ⁹ Yang, Q.-F., Yi, X., Yang, K. Y. & Vahala, K. Stokes solitons in optical microcavities. *Nature Physics* **13**, 53–57 (2017).
 - ¹⁰ Spencer, D. T. *et al.* Towards an integrated-photonics optical-frequency synthesizer with <1 Hz residual frequency noise. In *Optical Fiber Communication Conference, M2J.2* (2017).
 - ¹¹ Suh, M.-G., Yang, Q.-F., Yang, K. Y., Yi, X. & Vahala, K. J. Microresonator soliton dual-comb spectroscopy. *Science* **354**, 600–603 (2016).
 - ¹² Dutt, A. *et al.* On-chip dual comb source for spectroscopy. *arXiv preprint arXiv:1611.07673* (2016).
 - ¹³ Pavlov, N. *et al.* Soliton dual frequency combs in crystalline microresonators. *Optics Letters* **42**, 514–517 (2017).
 - ¹⁴ Papp, S. B. & Diddams, S. A. Spectral and temporal characterization of a fused-quartz-microresonator optical frequency comb. *Physical Review A* **84**, 053833 (2011).
 - ¹⁵ Li, Q. *et al.* Stably accessing octave-spanning microresonator frequency combs in the soliton regime. *Optica* **4**, 193–203 (2017).
 - ¹⁶ Pfeiffer, M. H. *et al.* Octave-spanning dissipative Kerr soliton frequency combs in Si₃N₄ microresonators. *arXiv preprint arXiv:1701.08594* (2017).
 - ¹⁷ Luke, K., Okawachi, Y., Lamont, M. R., Gaeta, A. L. & Lipson, M. Broadband mid-infrared frequency comb generation in a Si₃N₄ microresonator. *Optics Letters* **40**, 4823–4826 (2015).
 - ¹⁸ Savchenkov, A. A. *et al.* Generation of Kerr combs centered at 4.5 μm in crystalline microresonators pumped with quantum-cascade lasers. *Optics Letters* **40**, 3468–3471 (2015).
 - ¹⁹ Yu, M., Okawachi, Y., Griffith, A. G., Lipson, M. & Gaeta, A. L. Mode-locked mid-infrared frequency combs in a silicon microresonator. *Optica* **3**, 854–860 (2016).
 - ²⁰ Hugi, A., Villares, G., Blaser, S., Liu, H. & Faist, J. Mid-infrared frequency comb based on a quantum cascade laser. *Nature* **492**, 229–233 (2012).
 - ²¹ Ludlow, A. D., Boyd, M. M., Ye, J., Peik, E. & Schmidt, P. O. Optical atomic clocks. *Reviews of Modern Physics* **87**, 637 (2015).
 - ²² Nez, F., Biraben, F., Felder, R. & Millerioux, Y. Optical frequency determination of the hyperfine components of the 5S_{1/2}-5D_{3/2} two-photon transitions in rubidium. *Optics Communications* **102**, 432–438 (1993).
 - ²³ Papp, S. B. *et al.* Microresonator frequency comb optical

- clock. *Optica* **1**, 10–14 (2014).
- ²⁴ Lee, S.-J., Widiyatmoko, B., Kourogı, M. & Ohtsu, M. Ultrahigh scanning speed optical coherence tomography using optical frequency comb generators. *Japanese Journal of Applied Physics* **40**, L878 (2001).
- ²⁵ Kray, S., Spöler, F., Först, M. & Kurz, H. Dual femtosecond laser multiheterodyne optical coherence tomography. *Optics Letters* **33**, 2092–2094 (2008).
- ²⁶ Bajraszewski, T. *et al.* Improved spectral optical coherence tomography using optical frequency comb. *Optics Express* **16**, 4163–4176 (2008).
- ²⁷ Saha, K. *et al.* Broadband parametric frequency comb generation with a 1- μm pump source. *Optics Express* **20**, 26935–26941 (2012).
- ²⁸ Xue, X. *et al.* Second-harmonic-assisted four-wave mixing in chip-based microresonator frequency comb generation. *Light: Science & Applications* **6**, e16253 (2017).
- ²⁹ Jung, H., Stoll, R., Guo, X., Fischer, D. & Tang, H. X. Green, red, and IR frequency comb line generation from single IR pump in AlN microring resonator. *Optica* **1**, 396–399 (2014).
- ³⁰ Wang, L. *et al.* Frequency comb generation in the green using silicon nitride microresonators. *Laser & Photonics Reviews* **10**, 631–638 (2016).
- ³¹ Savchenkov, A. *et al.* Kerr combs with selectable central frequency. *Nature Photonics* **5**, 293–296 (2011).
- ³² Yang, Y. *et al.* Four-wave mixing parametric oscillation and frequency comb generation at visible wavelengths in a silica microbubble resonator. *Optics Letters* **41**, 5266–5269 (2016).
- ³³ Hausmann, B., Bulu, I., Venkataraman, V., Deotare, P. & Lončar, M. Diamond nonlinear photonics. *Nature Photonics* **8**, 369–374 (2014).
- ³⁴ Riemensberger, J. *et al.* Dispersion engineering of thick high-Q silicon nitride ring-resonators via atomic layer deposition. *Optics Express* **20**, 27661–27669 (2012).
- ³⁵ Okawachi, Y. *et al.* Bandwidth shaping of microresonator-based frequency combs via dispersion engineering. *Optics Letters* **39**, 3535–3538 (2014).
- ³⁶ Liu, Y. *et al.* Investigation of mode coupling in normal-dispersion silicon nitride microresonators for Kerr frequency comb generation. *Optica* **1**, 137–144 (2014).
- ³⁷ Ramelow, S. *et al.* Strong polarization mode coupling in microresonators. *Optics Letters* **39**, 5134–5137 (2014).
- ³⁸ Grudinin, I. S. & Yu, N. Dispersion engineering of crystalline resonators via microstructuring. *Optica* **2**, 221–224 (2015).
- ³⁹ Yang, K. Y. *et al.* Broadband dispersion-engineered microresonator on a chip. *Nature Photonics* **10**, 316–320 (2016).
- ⁴⁰ Oh, D. Y. *et al.* Coherent ultra-violet to near-infrared generation in silica ridge waveguides. *Nature Communications* **8**, 13922 (2017).
- ⁴¹ Kippenberg, T. J., Spillane, S. M. & Vahala, K. J. Kerr-nonlinearity optical parametric oscillation in an ultrahigh-Q toroid microcavity. *Physical Review Letters* **93**, 083904 (2004).
- ⁴² Moss, D. J., Morandotti, R., Gaeta, A. L. & Lipson, M. New CMOS-compatible platforms based on silicon nitride and Hydex for nonlinear optics. *Nature Photonics* **7**, 597–607 (2013).
- ⁴³ Xiong, C. *et al.* Aluminum nitride as a new material for chip-scale optomechanics and nonlinear optics. *New Journal of Physics* **14**, 095014 (2012).
- ⁴⁴ Lee, H. *et al.* Chemically etched ultrahigh-Q wedge-resonator on a silicon chip. *Nature Photonics* **6**, 369–373 (2012).
- ⁴⁵ Yang, K. Y. *et al.* Integrated ultra-high-Q optical resonator. *ArXiv e-prints* (2017). 1702.05076.
- ⁴⁶ Milián, C., Gorbach, A. V., Taki, M., Yulin, A. V. & Skryabin, D. V. Solitons and frequency combs in silica microring resonators: Interplay of the Raman and higher-order dispersion effects. *Physical Review A* **92**, 033851 (2015).
- ⁴⁷ Karpov, M. *et al.* Raman self-frequency shift of dissipative Kerr solitons in an optical microresonator. *Physics Review Letters* **116**, 103902 (2016).
- ⁴⁸ Yi, X., Yang, Q.-F., Yang, K. Y. & Vahala, K. Theory and measurement of the soliton self-frequency shift and efficiency in optical microcavities. *Optics Letters* **41**, 3419–3422 (2016).
- ⁴⁹ Cai, M., Painter, O. & Vahala, K. J. Observation of critical coupling in a fiber taper to a silica-microsphere whispering-gallery mode system. *Physics Review Letters* **85**, 74–77 (2000).
- ⁵⁰ Spillane, S. M., Kippenberg, T. J., Painter, O. J. & Vahala, K. J. Ideality in a fiber-taper-coupled microresonator system for application to cavity quantum electrodynamics. *Physics Review Letters* **91**, 043902 (2003).
- ⁵¹ Yi, X., Yang, Q.-F., Yang, K. Y. & Vahala, K. Active capture and stabilization of temporal solitons in microresonators. *Optics Letters* **41**, 2037–2040 (2016).
- ⁵² Stone, J. R. *et al.* Initiating Kerr-soliton frequency combs apart from thermal bistability and mode perturbation effects. In *Conference on Lasers and Electro-Optics*, STu4J.4 (2017).
- ⁵³ Miller, S. A. *et al.* Tunable frequency combs based on dual microring resonators. *Optics Express* **23**, 21527–21540 (2015).
- ⁵⁴ Dai, D. & Bowers, J. E. Novel concept for ultracompact polarization splitter-rotator based on silicon nanowires. *Optics Express* **19**, 10940–10949 (2011).